An initial evaluation of the thermodynamic or kinetic separation performance of cation-exchanged LTA zeolites for mixtures of propane and propylene

Mohammed-El Amine Benchaabane, Gabriel Trierweiler Gonçalves, Emily Bloch, Jean-Louis Paillaud, T. Jean Daou, Sandrine Bourrelly, Gérald Chaplais, Philip Llewellyn

An initial evaluation of the thermodynamic or kinetic separation performance of cation-exchanged LTA zeolites for mixtures of propane and propylene

Mohammed-El Amine Benchaabane [a], Gabriel Trierweiler Gonçalves [b,c], Emily Bloch [a], Jean-Louis Paillaud [b,c], T. Jean Daou [b,c], Sandrine Bourrelly [a,*], Gérald Chaplais [b,c], Philip L. Llewellyn [d]

[a] *Aix Marseille Univ, CNRS, MADIREL, UMR7246, F-13397, Marseille, France*
[b] *Université de Haute-Alsace, CNRS, IS2M, UMR 7361, F-68100, Mulhouse, France*
[c] *Université de Strasbourg, France*
[d] *TotalEnergies, OneTech, Centre Scientifique et Technique Jean Féger, Pau, France*

To cite this article: An initial evaluation of the thermodynamic or kinetic separation performance of cation-exchanged LTA zeolites for mixtures of propane and propylene*, Microporous Mesoporous Mater.* **2022***,* 344*,* 112211. DOI : 10.1016/j.micromeso.2022.112211*,* HAL : hal-03826143.
Received 14 July 2022; Received in revised form 28 August 2022; Accepted 3 September 2022; Available online 16 September 2022

Keywords*:* Adsorption, LTA type Zeolites, propylene/propane separation, calorimetry, IAST

ABSTRACT: Adsorptive separation of propylene (C_3H_6) and propane (C_3H_8) may represent an energy-efficient alternative to conventional cryogenic distillation. In this perspective, a set of zeolitic adsorbents of LTA type structure (puresilica zeolite (Si-LTA) and cation- (Na^+, 33% of Li^+, 50% of Mg^{2+} and 50% of Ca^{2+}) containing zeolites) were prepared, then characterized using various techniques such as PXRD, gas adsorption measurement, TGA, XRF, SEM and EDX mapping. Thanks to an in-house manometric dosing setup coupled with a Tian-Calvet type microcalorimeter, the pure gas adsorption isotherms and their corresponding differential enthalpies of adsorption were measured at 303 K and for pressures up to 5 bar. To fit those adsorption data, the dual-site Langmuir was selected as the best fit model, and by using the Ideal Adsorbed Solution Theory (IAST), thermodynamic selectivities were determined. The mass transfer constants were also estimated by fitting, separately, the Linear Driving Force (LDF) and isothermal micropore diffusion models to adsorption kinetic curves, thus allowing kinetic type selectivities to be calculated. The combination of those selectivities reveals that the thermodynamic separation of C_3H_6 from C_3H_8 is highly favorable on CaNa-LTA, followed by its MgNa-LTA counterpart with IAST selectivities around 15 and 5, respectively. On the other hand, the monovalent cationic zeolites (i.e., Na- and LiNa-LTA) show a predominance of steric effects. Also, except for Si-LTA which shows a moderate kinetic separation, the studied materials are potential candidates, in the following order CaNa- > MgNa- > LiNa- > Na-LTA, for the separation of C_3H_6 from C_3H_8 by adsorption-based technologies.

1. INTRODUCTION

Separation of a binary mixture of propane (C_3H_8) and propylene (C_3H_6) is of great commercial importance in petrochemical industries, since the separated propylene is considered as a raw material of the wide variety of valuable products. One of the most important being as a monomer feedstock for polypropylene production, the world's secondmost widely produced synthetic plastic; for which a high purity of at least 99.5% (mol) is required [1]. The propylene demand growth rate is over 6% per year in the last five years and it is forecast to further worldwide grow [2]. Currently, C_3H_6/C_3H_8 separation is performed by cryogenic distillation (operation at low temperatures and high pressures [3,4]) using a huge splitter column of over 100 trays along with a very high reflux ratio [1,4–6]. Undoubtedly, this heat-driven process is capital and highly energy-intensive, owing to the high similarity between both hydrocarbon molecules in terms of relative volatilities and kinetic diameters. Therefore, finding energy-efficient alternatives to this traditional separation technique means looking for more tunable procedures, such as selective adsorption based-processes [7–9], where their performance substantially depends on the chemical properties and structure characteristics of the implemented porous materials [10,11].

From an industrial scale-up point of view, adsorption phenomena appear in Pressure Swing Adsorption (PSA) or Vacuum Swing Adsorption (VSA) plants; where many adsorption/desorption cycles run in a quasi-continuous regime to offer an enriched flow product [9,12–14]. Such adsorption based-installations, in which the main part is the design of an efficient adsorbent [15], stand out as the most attractive techniques, simply because of possible high selectivities and high capacities towards propylene obtained under mild operating conditions (ambient temperature and atmospheric pressure, and even in low partial pressure domain). Thereby, compared with distillation, adsorptive separations using adequate porous materials tends to be an energy- and a cost-effective strategy [11,16,17].

Many adsorbents have been reported in the open literature for the separation of propane and propylene, including all type of zeolites [1,4, 18], silica gels [19], and carbon molecular sieves (CMCs) [20,21]. Other inorganic silica-containing adsorbents such as Si-CHA [22],

DD3R [15], SBA-15 [23] and MCM-41 have been synthesized and evaluated as well as emerging hybrid structures, e.g., metal-organic frameworks [24][–][26]. On the other hand, several studies on π-complexing agents (with either copper or silver ions) containing materials have been carried out [4,27–30]; however, it is of great worth to note that one of the potential challenges hampering the large-scale application of π-complexation-based processes is the deactivation of the complexing agents (reduction of Ag^+ or disproportionation of Cu^+) after long-term usage [31,32]. For the zeolitic adsorbents family, some interesting studies can be mentioned in further detail: Olson et al. [33] noted that zeolites having 8-member rings together with no acidity or acid activity that does not polymerize olefins are preferred. In that work, they stated that ion-exchanged process with low activity metal cations can be used for the control of acidity; preferred cations are alkali metal cations, while larger cations are attractive for faster desorption of the desired olefin. The same authors reported [33] that CHA and ITE-type structures are preferable zeolites for the kinetic separation of C_3H_6/C_3H_8 mixture. More recently, DD3R zeolite, as a pure-silica zeolite, has been proposed as a desirable choice, capable of kinetically separate propylene from propane [15,34]. On the reported synthesis of LTA in pure silica form, Si-LTA (also named ITQ-29), by Corma et al. [35], only the adsorption equilibrium and kinetics of methane, ethane, ethylene, and propylene were investigated using PFG NMR technique [36].

Regarding polar zeolites, Da Silva and Rodrigues [18] studied adsorption equilibria and kinetics of propylene and propane over commercial 13× and 4 A zeolites at temperatures between 373 and 473 K and up to 1 bar. It was established [18] that the 13× zeolite shows a higher loading capacity and lower mass-transfer resistance, whereas the 4 A zeolite shows the highest selectivity for propylene. Subsequently, Padin et al. [30] pointed out that the 4 A (NaA) zeolite is capable of selectively adsorbing propylene over propane, although it has a slow propylene uptake, and with 95% Li^+ cations (NaLiA) this zeolite showed the optimal characteristics for the kinetic separation of a propane/propylene mixture. In the same study, they stated that an aluminophosphate (AlPO4-14) zeolite is able to sterically exclude propane. In an attempt to improve the olefin/paraffin separation capability of NaX, Grande et al. [37] exchanged Li^+ (ion exchange of an 80%) into the framework and studied gas adsorption behavior of the resultant zeolite. The difference in loading between both gases is larger for the lithium-exchanged product than the precursor, while the gas adsorption kinetics remain basically unchanged. Divekar et al. [38] systematically compared the propylene/propane separation performance of 13×(Z10-04, Zeochem), 5 A (UOP) and laboratory-made Na-ETS-10. Ideal adsorbed solution theory (IAST) predicted that Z10-04 possesses the highest propylene/propane selectivity exceeding 20 for pressure valuegreater than 1 bar, whereas 5 A and Na-ETS-10 samples show moderate and similar selectivity values of ~8 at 423 K and 298 K, respectively.

Interestingly, these wide variety of porous solids can be categorized into three types of separation mechanisms: equilibrium separation, steric separation (size exclusion or molecular sieving), and kinetic separation. In equilibrium separation, the separation is based on difference of affinities between adsorbent and adsorbates. In this case, no attempt has been made so far to directly measure the enthalpy of adsorption, only and in some cases the isosteric heats calculated by the familiar Clausius-Clapeyron expression are given. In contrast, kinetic mechanism takes the lead when adsorption rates of the diffusional molecules are different. Lastly, strong steric effects could be interpreted as the limit of kinetic separations [39].

Therefore, in this present work, the main objective is to study the potential of four adsorbents, namely, pure-silica zeolite (Si-LTA also known as ITQ-29), whose framework is neutral and some cationic zeolites: Na-LTA and its exchanged zeolitic forms (LiNa-with 33% of Li^+, CaNa- and MgNa-LTA with 50% of Ca^{2+} and Mg^{2+} in each), for an efficient separation of propylene from propane. To this end, kinetics and adsorption equilibrium measurements for propane and propylene on those sorbents were described, and for the first time the pseudo differential enthalpies of adsorption were measured at 303 K and up to 5 bars. Afterwards, various models have been adopted for correlation of isotherm data with the view to estimate the IAST (Ideal Adsorbed Solution Theory) selectivity of those adsorbents towards propylene.

2. Experimental section

2.1 Reagents and materials

NaA (LTA) in powder form, provided by Aptar CSP Technologies (Niederbronn-Les Bains, France), was used as starting material to perform the cationic exchanges. The metal salts, lithium chloride (LiCl, Alfa Aesar ≥ 99%), calcium chloride hexahydrate ($CaCl_2{\cdot}6H_2O$, Riedelde Haën ≥99%), and magnesium chloride hexahydrate ($MgCl_2{\cdot}6H_2O$, Roth ≥99%) were used as cation sources during the cationic exchange processes. Boric acid (H_3BO_3, Acros Organic/Thermo Fischer Scientific ≥99.5%) was used as binder during X-ray Fluorescence analyses. Cationic exchanges were performed following the procedure described by Tahraoui et al. [40]. Na^+ cations were exchanged by Mg^{2+} cations in NaA by mixing the starting zeolite with 1 M aqueous solution of magnesium chloride for 2 h at 80 °C under stirring, keeping a fixed ratio of 1 g zeolite to 20 mL solution. After that, the suspension was filtered and the solid was washed under sonication (3 min) with four portions of 200 mL of deionized water. Finally, the solid was dried at 80 °C overnight. The same procedure was repeated using the same molar concentration of aqueous solution of lithium chloride in order to exchange Na^+ cations by Li^+ cations. Similarly, by using 0.1 M aqueous solution of calcium chloride, the Na^+ cations were also exchanged by Ca^{2+} cations. The exchanged zeolites were named MgNa-LTA and CaNa-LTA and LiNa-LTA.

Pure-silica LTA zeolite was prepared according to the protocol based on seeding route and described by Bouizi et al. [41]. The reactants used were tetraethylortosilicate (Fluka 98%), tetramethylammonium hydroxide ($TMAOH{\cdot}5H_2O$, Aldrich), hydrofluoric acid (Carlo

Erba 40%), distilled water, and 2,3,6,7-tetrahydro-1*H*,5*H*-pyrido[3,2,1-ij]quinolone (julolidine, Sigma-Aldrich 97%), which was quaternarized with an excess of methyl iodide (purum, Sigma-Aldrich ≥ 99.0%) into 4-methyl-2,3,6,7-tetrahydro-1*H*,5*H*-pyrido[3.2.1-ij]quinolinium iodide and then converted into its hydroxide form (MJulOH) by ion exchange (Amberlite IRA 400, Sigma-Aldrich) following the protocol of Corma et al. [35]. The reagents were mixed, resulting in a gel of molar composition: 1 SiO_2: 0.25 MJulOH: 0.25 TMAOH: 0.5 HF: 5H_2O: 0.02 LTA seeds (Si/Al = 1). The gel was transferred into an PTFE-lined stainless-steel autoclave which was further heated at 135 ◦C for 48 h. The resulting solid was washed and dried overnight at 70 °C. A second synthesis was then performed following the same procedure but using the zeolite obtained after the first synthesis (Si/Al = 50) as seed source. The resulting nearly pure-silica LTA zeolite (Si/Al > 1000) was washed with deionized water and dried overnight at 70 °C before being calcined in air at 650 °C for 12 h.

2.2 General characterization

Powder X-Ray diffraction (PXRD) patterns of the samples were recorded on a PANalytical MPD X'Pert Pro diffractometer operating with Cu Kα radiation (Kα = 0.15418 nm) equipped with an PIXcel realtime multiple strip detector (active length = 3.347° 2θ). The XRD patterns were collected at 22 °C in the 3° < 2θ < 50° range, by step of 0.013° in 2θ and with a time of 220 s by step.

X-ray Fluorescence (XRF) analyses were performed using an X-Ray Fluorescence (XRF) spectrome-ter Zetium, 4 kW, PANalytical. Prior to the analyses, the samples were mixed with boric acid (binder). 200 mg of the sample were grinded with 100 mg of boric acid and pressed into 13 mm diameter pellets for 2 min at a pressure of 5 ton.

Scanning Electron Microscopy (SEM) images were recorded using a JSM-7900 F (JEOL, Ltd.) scan-ning electron microscope and Energy Dispersive X-rays Spectroscopy (EDX) maps were obtained by QUANTAX energy dispersive spectrometer equipped with two Xflash 6–30 detectors (BRUKER Nano, GmbH). Before analysis, the samples were coated with a fine carbon layer using a SCD004 sputter coating system (BAL-TEC, LEICA MICROSYSTEMES SA) in order to improve the electrical conductivity.

Thermogravimetric analyses (TGA) were performed on thermobalance, Q500, from (TA) instrument. Approximately 10–20 mg of adsorbent was placed in a platinum crucible and constantly weighed by a microbalance. This step was performed while the sample was heated from room temperature up to 800 °C at a heating rate of 5 °C.min^{-1}, and in inert atmosphere ensured by argon at a flow rate of 40 mL min^{-1}.

Textural properties were determined from nitrogen adsorption isotherms at 77 K measured with a 3-Flex Micromeritics analyzer. Before all the adsorption measurements, zeolite samples were evacuated under a secondary vacuum for 24 h at 623 K with a heating ramp of 1 °C. min^{-1}.

2.3 Isotherms, kinetics and adsorption microcalorimetry measurements

Adsorption microcalorimetry experiments at 303 K and for pressure up to 5 bar were performed using an in-house built setup that combines manometric dosing system with a high sensitivity Tian-Calvet isothermal type microcalorimeter [42]. This microcalorimeter consists of two thermopiles mounted in electrical opposition to compensate for spurious heat effects during dosing. Each thermopile comprises of around 1000 chromel-alumel thermocouples. This apparatus allows both the isotherms and the pseudo differential enthalpies of adsorption as a function of the coverage to be measured simultaneously. The errors in the isotherms can be considered as better than 5% and errors in the enthalpies are of ±1 kJ mol^{-1}.

In this study, the adsorption kinetics were measured during the adsorption process from the decrease of pressure which is recorded automatically as a function of time until reaching the equilibrate state. This data was used to calculate the adsorption amount in each time, Mt, on the basis of the difference between the initial amount of gas introduced into the cell and the amount of gas residual in the dead volume of the cell at any given time '*t*'. Additionally, the final adsorption amount, M_f, was calculated using the pressure of the adsorption cell at equilibrium pressure P ($t \rightarrow \infty$). Thus, the adsorption uptake, M_t/M_f, was obtained as a function of time. Then, by applying an appropriate diffusion model to the experimental collected data, the intracrystalline diffusivity (D_c) can be derived.

3. Theoretical section

3.1 Mathematical modeling of single-component adsorption isotherm

Many mathematical models have been suggested to describe physical adsorption of adsorbates on an adsorbent surface. In our work, we initially chose Langmuir, dual-site Langmuir (DSL), triple-site Langmuir (TSL) and Toth models [43–45] to correlate isotherm data for two reasons: first, these models can be reduced to Henry's law at infinitely dilute conditions. In other words, such models are thermodynamically consistent, and consequently the integration of the spreading pressure equation (given by equation (6)) between zero and any hypothetical pressure would be possible. Secondly, an analytical solution of the spreading pressure can be easily obtained for some of these model (i.e., Langmuir and Toth).

A comparison of goodness of fit of the aforementioned different models against the experimental isotherm data for Si-, MgNa- and CaNa-LTA with propylene and propane is shown in Fig. S3. The accuracy of each model fit to the experimental data is first judged by visual inspection and then quantified using both the nonlinear chi-square test (X^2) (1) and the correlation coefficient (R^2) (2), as given in Table S1. This table shows that the two-site Langmuir fitted model is the model that was able to provide a tard-off between an intermediate model complexity and high fitting procedure quality, and thus why it was selected for predicting IAST selectivity.

$$X^2 = \sum_{i=1}^{n} \frac{(n_{pred} - n_{meas})^2}{n_{meas}} \quad (1)$$

$$R^2 = \frac{\sum(n_{meas} - \bar{n}_{pred})^2}{\sum(n_{meas} - \bar{n}_{pred})^2 + \sum(n_{meas} - n_{pred})^2} \quad (2)$$

where n_{pred} is the equilibrium capacity obtained from the model, nmeas is the equilibrium capacity obtained from experimental data, and $\bar{n}_{pred}$ is the average of npred. Interestingly, since there were very large adsorption data points made in the low-pressure domain, equation (1) is biased toward the higher density of data at low adsorption amounts. This is of utmost importance because it allows to determine the limiting selectivity (i.e., the ratio of Henry's constants) with a fair accuracy.

3.1.1 *Dual Site Langmuir (DSL) isotherm*

The dual-site Langmuir model (DSL) is a good choice to describe heterogeneous adsorption [38]. Herein, the surface adsorbent heterogeneity is taken into account as the sum of different homogenous surfaces which contain equivalent energetic adsorption sites. In this model, adsorbate-adsorbate interactions are neglected, and the adsorbate-adsorbent free energy on each site is constant. Equation (3) represents the DSL isotherm.

$$n = \frac{n_{01} b_1 P}{1 + b_1 P} + \frac{n_{02} b_2 P}{1 + b_2 P} \quad (3)$$

where n is the amount adsorbed at pressure P; n_{Oi} and b_i are respectively the ultimate capacity and affinity parameter specific to each adsorption site (notations 1 and 2 are used to point out to two different adsorption sites).

Once the fitting procedure is complete, the fitted parameters of DSL model (as an output) for given adsorption data are obtained. By taking these estimated values (i.e., n_{oi} and b_i) as starting point, one can then determine the Henry's law constant, k_H, by the following expression [45]:

$$K_h = \sum_{i=1}^{2} K_{H,i} = \sum_{i=1}^{2} n_{0i} b_i \quad (4)$$

According to this, k_H is simply the sum of partial Henry's constants that correspond to multiple homogenous surfaces considered within the adsorbent, and when i = 1, equation (4) reduces systematically to unique Henry's constant that can readily be deduced from the conventional Langmuir model when P tends to zero.

3.1.2 *Ideal Adsorbed Solution Theory (IAST)*

From an application point of view, prediction of mixed gas adsorption from only pure component isotherms is undoubtedly much more convenient, rather their direct measurement of mixture equilibria that is complicated and time-consuming even for a binary system. In this regard, by far the most common used approach is the model developed by Myers and Prausnitz [46], so-called Ideal Adsorbed Solution Theory (IAST). This theory states that the behavior of the adsorbed phase is similar to that of an ideal solution, which is in thermodynamic equilibrium with a perfect gas phase, giving rise to an equilibrium equation analogous to Raoult's law for liquid-vapor equilibrium defined as follows:

$$P_i = x_i P_i^0(\pi); i = 1, 2, \cdots n \quad (5)$$

where P0i, is the equilibrium vapor pressure for every component i and xi is the mole fraction in the adsorbed phase, which can be expressed in terms of the total adsorbed amount nt, by:

$$\left(\frac{1}{n_t}\right) = \sum_{i=1}^{N} \frac{x_i}{n_i(P_i^0)} \quad (6)$$

where n_i, is the adsorbed amount of a pure compound. It can be represented by any isotherm model as a function of P_1.

Also, under the assumption in which the spreading pressure of the gas mixture, π, is equal to the spreading pressures for each component π_i, of the system, the following equation can be given:

$$\frac{A\pi}{RT} = \frac{A\pi_i}{RT} = \int_0^{P_i^0} \frac{n_i}{P_i} dP_i \quad (7)$$

where A represents the surface area per kg of framework and the $A\pi/RT$ (mol.kg^{-1}) corresponds to the adsorption potential [19]. The adsorption potential can be determined by analytic integration of the unary isotherm data fits for each component.

The use of the IAST (i.e., by solving the above set of equations (5)–(7) allows calculation of the adsorption selectivity (α1/2) **towards propylene from a propylene/propane mixture at a given total pressure,** P**, defined by**:

$$S_{IAST} = \alpha_{1/2} = \frac{X_1/X_2}{y_1/y_2} \quad (8)$$

where X_1 and y_1 are the molar fractions of propylene in the adsorbed and gas phase, respectively, and X_2 and y_2 are the corresponding molar fractions of propane. At the limit of zero pressure, the IAST selectivity becomes equal to the ratio of Henry's law constants for the pure compounds.

3.2 Determination of diffusion coefficients

The kinetics of propylene and propane adsorption is a crucial factor in the adsorbent evaluation for this industrially important separation. Thus, we measured propylene and propane adsorption as a function of time at 303 K utilizing the home-made manometric apparatus (described previously). Note that, to avoid over heating of the adsorbent bed, small gas amounts are introduced to the sample cell for these measurements.

In the literature, estimation of the diffusion coefficients of gases into microporous adsorbents have been extensively undertaken by fitting the experimental uptake curve ($M_t/M_f = f\ (t^{1/2})$ to the analytical solution of the model of transient diffusion with intracrystalline diffusion control (so-called Crank's model) [47,48]. The Crank's model, given by equation (9), is based on the following assumptions: (i) the adsorbent particles are spherical, uniform in size and density, and (ii) the system is isothermal with negligible pressure drop (linear isothermal system). This model, derived from Fick's Law, predicts fairly good diffusion coefficients in the case of systems with low concentration variations. In the short time region, the kinetic uptake curve is essentially linear and approximated by equation (10), whereas equation (11) is given for the long-time region.

Over the entire time range,

$$\frac{M_t}{M_f} = 1 - \frac{6}{\pi^2}\sum_{n=1}^{\infty}\frac{1}{n^2} exp\left(-n^2\pi^2\frac{D_c}{r_c^2}t\right) \quad (9)$$

where M_f and M_t are the adsorption amount of gas at the final or equilibrium state and at any given time t, respectively. D_c and r_c are referred to intracrystalline diffusivity and the equivalent spherical crystal radius, respectively.

If the adsorption time is short,

$$\lim_{t\to 0}\frac{M_t}{M_f} = \frac{6}{r_c}\sqrt{\frac{D_c t}{\pi}} \quad (10)$$

If the adsorption time is long,

$$\lim_{t\to 0}\frac{M_t}{M_f} = 1 - \frac{6}{\pi^2}\sum_{n=1}^{\infty}\frac{1}{n^2} e^{-\pi^2\frac{D_c}{r_c^2}t} \quad (11)$$

For purpose of comparison, and since the exact model, as an infinite series, is slowly convergent and computationally complex, the linear driving force (LDF) approximation with the (kLDF) rate constant, given by equation (12), was also employed in this work. It was

originally obtained by Glueckauf and Coates [49] for the surface diffusion mechanism with a constant diffusivity, that is, the diffusing molecules can never escape the force field of the adsorbent surface. It assumes that axial and radial diffusions in the fixed bed are negligible which is one of its weaknesses [50]. In this mechanism, the surface diffusivity coefficient is usually much smaller than the other diffusivities (macropore and film transfer resistances). This allows the mass transfer coefficient to be given by equation (13) [51].

$$\frac{\partial M_t}{\partial t} = k_{LDF}\left(M_f - M_t\right) \quad (12)$$

$$K_{LDF} = 15\,\frac{D_c}{r_c^2} \quad (13)$$

k_{LDF} is referred to as the mass transfer constant.

4. Results and discussion

4.1 A-zeolite adsorbents characterizations

The powder X-ray diffraction patterns of all LTA-type zeolites are plotted in Fig. 1. All diffractograms correspond to pure LTA cubic phase. The refined unit cell parameters in the space group *Fm*-3*c* were found to be *a* = 24.579(1) Å for the raw zeolite; *a* = 24.216(2) Å for sample LiNa-LTA; *a* = 24.591(1) Å for sample CaNa-LTA; and *a* = 24.397(3) Å for the sample MgNa-LTA. Compared to the raw zeolite, the unit cell parameters of CaNa-LTA barely vary upon exchange with Ca^{2+}, due to small difference of Na^{+} ionic radius (1.02 Å) and Ca^{2+} ionic radius (1.00 Å) considering a coordination number of 6 [52]. For sample MgNa-LTA, however, replacing Na^{+} by Mg^{2+} caused framework contraction due to the Mg^{2+} smaller ionic radius (0.72 Å). The same trend is observed while exchanging Na^{+} by Li^{+} cations, which possesses even smaller atomic radius (0.69 Å). The a unit cell parameter for Si-LTA is of 11.855 (2) Å (space group *Pm*3*m*) which corresponds to 23.710(3) Å for a face-centered super unit cell.

X-ray fluorescence analysis was used to determine the chemical composition of the raw zeolite and further to estimate the degree of exchange in the samples LiNa-LTA, CaNa-LTA and MgNa-LTA, exchanged with Li^{+}, Ca^{2+} and Mg^{2+}, respectively. The information issued from XRF analysis are disposed in Table 1. The Si/Al ratio, as expected, is found to be 1 for the raw zeolite framework [53]. Moreover, the Si/Al ratio remains constant upon exchange process, in which 33% of exchange degree was obtained after a single exchange for the sample LiNa-LTA, and 50% of exchange degree after a single exchange for both CaNa-LTA and MgNa-LTA samples.

SEM images of pure-silica LTA, raw Na-LTA zeolite as well as the samples exchanged with Li^{+}, Ca^{2+} and Mg^{2+} are shown in Fig. 2. Si-LTA (Fig. 2a) features cubic particles ranging from 1 to 3 µm, which is inherent to LTA-type zeolites. NaA crystals (Fig. 2b) with particle size ranging from 1 to 4 µm also features cubic morphology but with slightly truncated particles. It's worth to pointed out here that the remarked subtle difference in particle size and morphology for these two zeolites are expected to minorly impact the diffusion process, especially the time completion of equilibrium adsorption, as observed by S. Tanaka et al. [54] from the uptake curves of the adsorption of n-butanol by crystal-size-engineered ZIF-8 samples (0.060, 0.47, 2.1 and 88 µm) of slightly different morphologies.

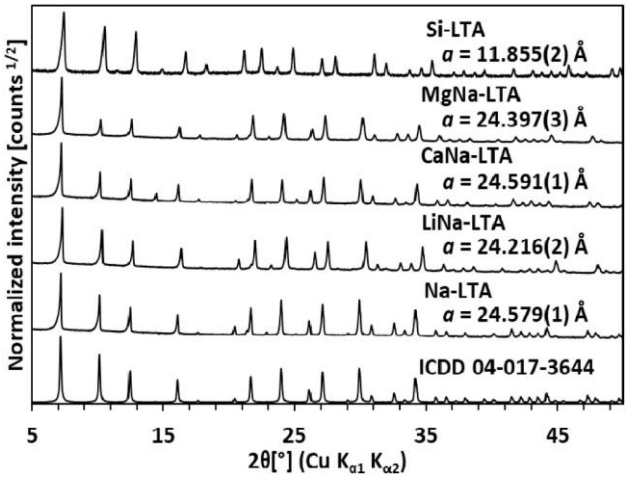

Figure 1. XRD patterns of ICDD 04-017-3644, Na-LTA, LiNa-LTA, CaNa-LTA, MgNa-LTA and Si-LTA.

For the rest of prepared zeolites, the cubic morphology remains intact and the particle size range does not vary throughout the exchanges with Ca^{2+} (Fig. 2c), Mg^{2+} (Fig. 2d), and Li^{+} (Fig. 2e). The sample exchanged with Mg^{2+} presents a sort of deposition over the crystal surface which was also observed by Tahraoui et al. [40] during its exchanges using Mg^{2+} cation. Bae et al. [55] purposely deposited magnesium hydroxide over MFI and LTA zeolites and obtained crystals with similar deposition pattern but with far more surface coverage.

Table 1
The physical properties of the LTA zeolites employed in propylene/propane separation.

Adsorbent	Anhydrous unit cell composition[a]	Degree of exchange (%)[b]	S_{BET} ($m^2.g^{-1}$)	Vp ($cm^3.g^{-1}$)	Dp (Å)
Si-LTA	$Si_{192}O_{384}$	No exchange	761	0.3	7.85
Na-LTA	$Na_{96}Al_{96}Si_{96}O_{384}$	No exchange	381[c]	0.20[c]	X[d]
LiNa-LTA	$Na_{64}Li_{32}Al_{96}Si_{96}O_{384}$	33	359[c]	0.17[c]	x[d]
CaNa-LTA	$Na_{48}Ca_{24}Al_{96}Si_{96}O_{384}$	50	700	0.26	7.83
MgNa-LTA	$Na_{48}Mg_{24}Al_{96}Si_{96}O_{384}$	50	702	0.27	7.83

[a] Determined by elemental analysis.

[b] Defined as (the number of Na^{+}, Li^{+}, Mg^{2+} or Ca^{2+} ions per unit cell)/(the sum of Al atoms per unit cell) × 100%.

[c] Determined from CO_2 adsorption measurements at 237 K.

[d] x refers to unknown values because the NLDFT model for the adsorption of CO_2 on carbons at 273 K is the only available model in our case.

Thus, this deposition can be attributed to the formation of magnesium hydroxide on the surface, even though it was not detectable in the PXRD. Moreover, the sample exchanged with Mg^{2+} displays a slightly overestimated exchange ratio value since the XRF analysis concerned the bulk, not distinguishing the fraction of the true exchange and the amount of the deposition at the surface of the crystals.

EDX mapping was performed over the exchanged samples in order to determine the atomic distribution (Al, Si, Na and Ca/Mg) and is shown in Fig. 3. EDX mapping is a useful tool to observe whether the cationic distribution is performed uniformly along the crystals, by comparing the decrease in color intensity of Na mapping (represented by the color yellow) accompanied by the increase in color intensity of the compensating cation Ca mapping (represented by the color pale green) and Mg mapping (represented by the color red). However, this technique is limited regarding Li+ cation due to its lightness, which prevents it to be detected during EDX analysis. EDX mapping performed in both samples CaNa-LTA (Fig. 3a and b) and MgNa-LTA (Fig. 3c and d) supports the XRF analysis findings as it shows the accomplishment of the cationic exchange process, confirmed by the emergence of pale green color (Fig. 3b) and red color (Fig. 3d), attributed to the presence of Ca^{2+} and Mg^{2+} cations in their respective samples. Moreover, EDX mapping of Ca and Mg shows a uniform distribution of Ca2+ cations for sample CaNa-LTA and of Mg2+ cations for sample MgNa-LTA, confirming the cationic homogeneous dispersion along the crystals.

The comparison of the TGA profiles from the A-zeolite samples is shown in Fig. 4. Great thermal stability up to 800 ◦C is observed. For the Type A cationic zeolites, two main different temperature regions of water loss are observed; the first weight loss is located in the temperature range of 80–130 °C, which can be ascribed to physically adsorbed water molecules in the outer surface while the second weight loss, occurred around 200 °C, is attributed to the strongly adsorbed water to extra-cations present within their porous structure [56]. In contrast to those zeolites, the pure-silica zeolite (Si-LTA) manifests a negligible weight loss (ca. 1%) because of its neutral framework.

The nitrogen (N_2) adsorption isotherms measured at 77 K are displayed in Fig. 5a. According to the IUPAC classification, those adsorption isotherms resemble to type I isotherm typical of microporous adsorbents, except for the zeolite Na-LTA and its partially Li-exchanged counterpart, which were further characterized by carbon dioxide (CO_2) because the N_2 molecules cannot pass through their pore apertures size. The CO_2 adsorption isotherms measured at 273 K are thus presented in Fig. 5b.

From the exploitation of all adsorption isotherms, the following textural properties were determined and summarized in Table 1: the equivalent specific surface area, S_{BET}, by the Brunauer-Emmett-Teller (BET) theory [57]; the total pore volume (in our case equal to micropore volume), Vp, was estimated by the t-plot method [44]; the micropore size distribution (PSD) of the studied samples was performed by applying the Density Functional Theory (DFT) [58] models on the collected N_2 adsorption data utilizing AsiQWin software of Autosorb-IQ (Quantachrome Instruments). Due to the non-availability of DFT models adapted to CO_2 adsorption on zeolites, the PSD from the measured CO_2 isotherms on the monovalent zeolites were not calculated. Therefore, in Fig. S1, only the PSD for porous zeolites measured with N_2 at 77 K are shown. The pore diameter corresponding to the maximum of PSD is denoted as Dp, where their corresponding values are disposed in Table 1. They were found to be almost identical (around 7.8 Å) and being higher than their respective theoretical pore aperture size (around 4.4 Å for Si-LTA and 5 Å for the divalent cation-containing zeolites discussed in more detail in

section 4.3). This can be explained by the continuous filling of the windows and cages of the zeolites of interest, yielding in PSD centered on a pore size (Dp) intermediate between that of the windows and cages. In Fig. S2, the comparison of accuracy between the isotherm predicted by the DFT model and the experimental isotherm is shown for each zeolite. In all cases, the applied DFT models were able to reproduce very accurately the experimental adsorption isotherms.

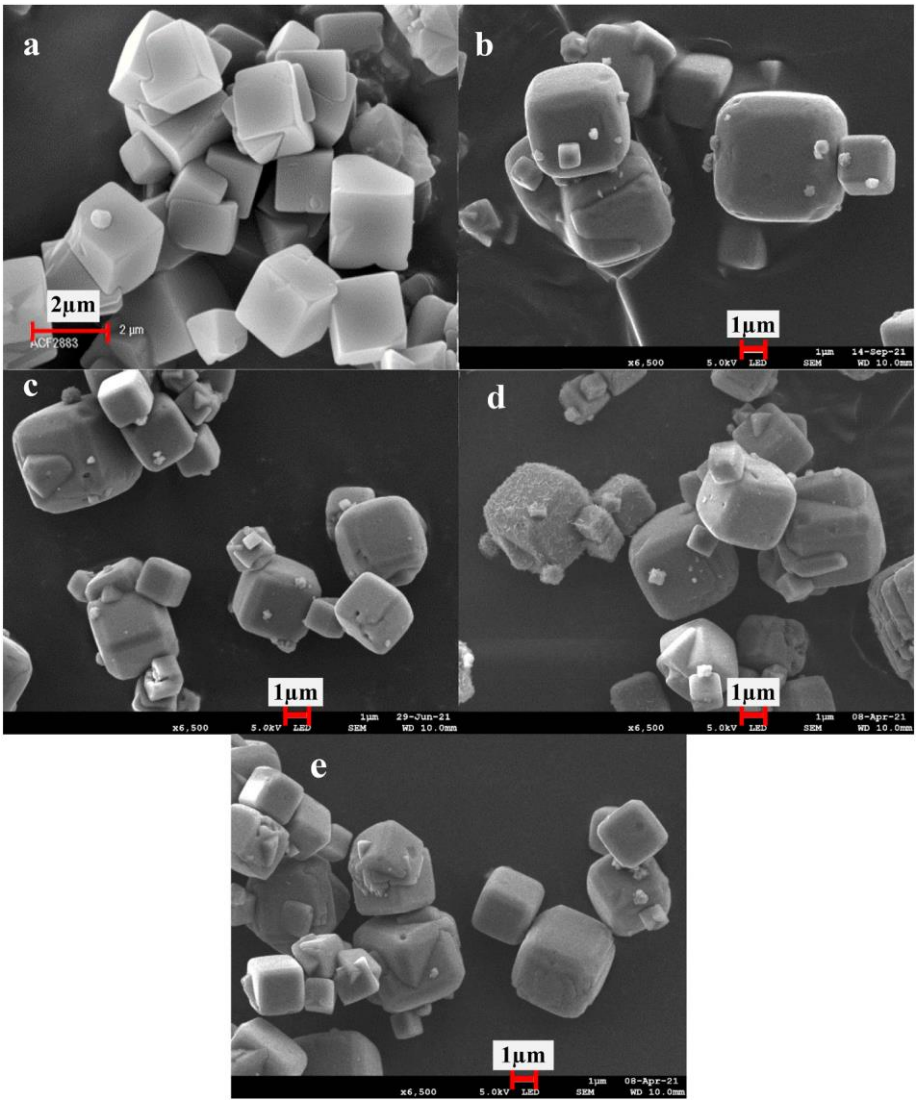

Figure 2. SEM images of (a) Si-LTA; (b) Na-LTA; (c) CaNa-LTA; (d) MgNa-LTA; (e) LiNa-LTA.

As can be seen in Table 1, most of prepared samples (Si-, CaNa- and MgNa-LTA) have comparable textural properties, but substantially different (being higher) from those determined for the monovalent cationic synthesized zeolites (i.e., Na- and LiNa-LTA). Indeed, this is a direct consequence of the duality between two factors that are the cation valence and its related distribution within the porous zeolite structure. By replacing the monovalent cation with the divalent one, more volume space can be generated as a result of decreasing the number of compensating cations of well-defined positioning.

4.2 Adsorption isotherm measurements

Fig. 6 shows the experimentally measured propane and propylene isotherms data for Si-, MgNa- and CaNa-LTA zeolites at 303 K and pressures up to 5 bar along with the best-fit DSL isotherm equation curves. The data in the left panel is plotted on a linear scale, while the same data in the right panel is plotted on a logarithmic scale. The latter plot is very useful as it allows to explore the microporosity of the adsorbents. The DSL model matches both the slope and magnitude of the measured data at low pressures, as seen in the logarithmic scale plot (Fig. 6). DSL fitted parameters are given in Table S2.

All the isotherms in Fig. 6 display a sharp uptake at low pressure. According to the figure, precisely where the isotherms data for CaNa- and MgNa-LTA are plotted in a semi logarithmic scale, it can be seen that propylene is more adsorbed than propane. However, this is not the case for the pure-silica zeolite 'Si-LTA', whose propylene and propane uptakes are almost the same up to 0.15 bar. Also, note that more propylene molecules can be packed within the pore structure of Si-LTA zeolite at high pressure (2.7 mmol g^{-1} for propylene vs. 2.5 mmol g^{-1} for propane at 5 bar) since propylene molecules are smaller than propane (42 g mol^{-1} vs. 44 g mol^{-1} for propylene and propane respectively). This implies that Si-LTA zeolite is not an effective adsorbent to separate thermodynamically propylene from propane, contrary to what was observed in the case of CaNa- and MgNa-LTA samples. As evident from Fig. 6, the propylene saturation capacities of MgNa-LTA and CaNa-LTA are nearly the same. This result is confirmed by the comparable values of BET surface area and specially micropore volume reported in Table 1. While the percentage of the bivalent cations are the same, this may be attributed to the smaller radius of Mg^{2+} cations compared to that of Ca^{2+} cations.

As noticed from Table 1, although Si-LTA zeolite has the highest micropore volume, the amount adsorbed of propylene and propane estimated at 5 bars were found to be low as compared to those for CaNa- and MgNa-LTA zeolites. This is probably due to adsorption isotherms that did not yet reach the adsorption completion of pore-filling regime at the highest measured pressure of 5 bar (Fig. 6). On the other hand, the propylene uptakes of Na-LTA and its Li-exchanged form at 303 K and 5.0 bars are lower than for Ca^{2+}- and Mg^{2+} -exchanged forms of Na-LTA. This is not unexpected because the number of extra-framework cations per unit cell is larger in the former materials than in the latter materials (Table 1).

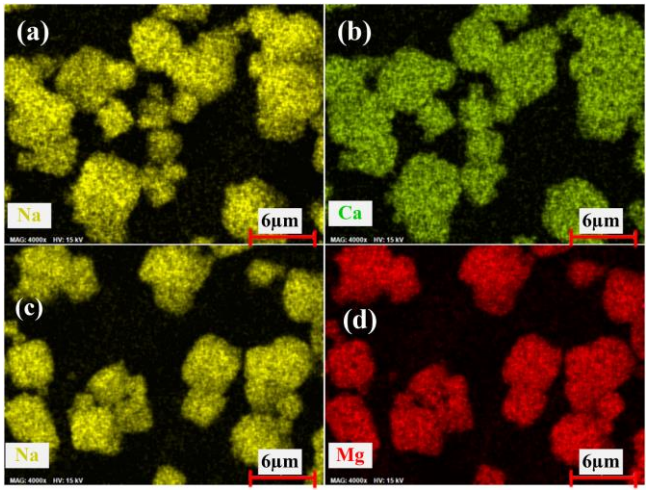

Figure 3. EDX mapping of Na and compensating cation for (a, b) CaNa-LTA and (c, d) MgNa-LTA.

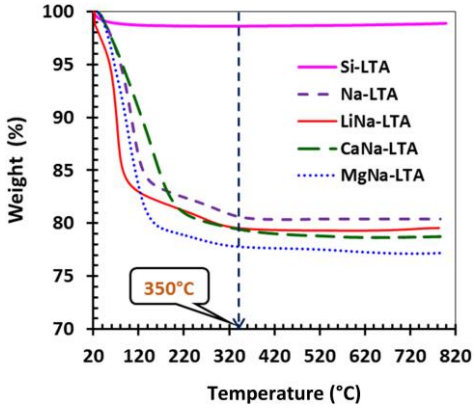

Figure 4. TGA curves for Si-LTA, Na-LTA, LiNa-LTA, CaNa-LTA and MgNa-LTA obtained with high resolution mode in argon at 5 K min^{-1}.

In the case of Na-LTA and its partially Li-exchanged counterpart (LiNa-LTA), while the propylene adsorption isotherm is characterized as Langmuir type I, the propane isotherm adopts somewhat a linear to steep shape with a low uptake (0.1 mmol g^{-1} for Na-LTA against ≃ 0.3 mmol g^{-1} for LiNa-LTA) at 303 K and 1.0 bar (see Fig. S4). It seems that C_3H_8 is essentially excluded from entering the pore structure of Na- and LiNa-LTA zeolites, whereas the C3H6 molecules are free to diffuse. This adsorption behavior appears to be

typical to a molecular sieve effect. However, this not the case since the experimentally measured isotherms for propane on these adsorbents did not reach the equilibrium state even after almost seven days at 303 K meaning that propane still adsorbs but very slowly (see Fig. S6). Another remarkable observation from Fig. S3 can be made: unlike Si-LTA, CaNa-LTA and MgNa-LTA, propylene isotherm for Na-LTA is very rectangular shaped, this may be explained by a combination of strong adsorptive interactions and the effective aperture size 3.8 Å [4] very close to the kinetic diameter of the C_3H_6 molecules (3.6 Å) [59]. Propylene capacities at equilibrium at 1 bar reported by Da Silva and Rodrigues [18] on a commercial Na-LTA Zeolite (Rhône-Poulenc) (1.9 mmol g^{-1} at 303 K) and by Järvelin and Fair [1] on an extrudate Na-LTA (2 mmol g^{-1} at 298 K) are slightly lower than that of our synthesized Na-LTA sample (2.9 mmol g^{-1} at 1.0 bar and 303 K). As expected, this suggests that the nature and amount of binder in these shaped/pelletized zeolites can affect its isotherm capacity.

4.3 Uptake measurements of propylene and propane on zeolites

Careful assessment of the performance of an adsorbent should consider an estimation of the diffusion coefficient of the gas molecules from the bulk gas phase into the pores of the adsorbent. Thus, the fractional uptake curves of propane and propylene on Na-LTA and their Li-, Ca-, Mg- exchanged forms and Si-LTA samples were measured experimentally at 303 K by dosing 0.1 bar of propylene and propane, separately, from a reservoir to each adsorbent. The results are shown in Fig. 7. Experimental data of propylene and propane adsorption kinetics were fitted by both Crank's model (8) and LDF model (9). As can be seen, the kinetic uptake data are well described by these two models (R^2 > 0.9) (see Figs. S10–S13). The fitting kinetic rate constants of Crank's model together with linear driving force model, LDF, for all the studied adsorbents are listed in Table 2. They are of the same order of magnitude with deviations smaller than 20%, occur with more important differences in the case of Si-LTA. This may be ascribed to the existence of other mass transfer resistances (macroporous and/or external film diffusion) rather than purely micropores resistance since the LDF model considers all type of diffusivity in a consolidated kinetic coefficient. So, the comparison between the two diffusion model solutions is important in the way that the reliability of our findings increases.

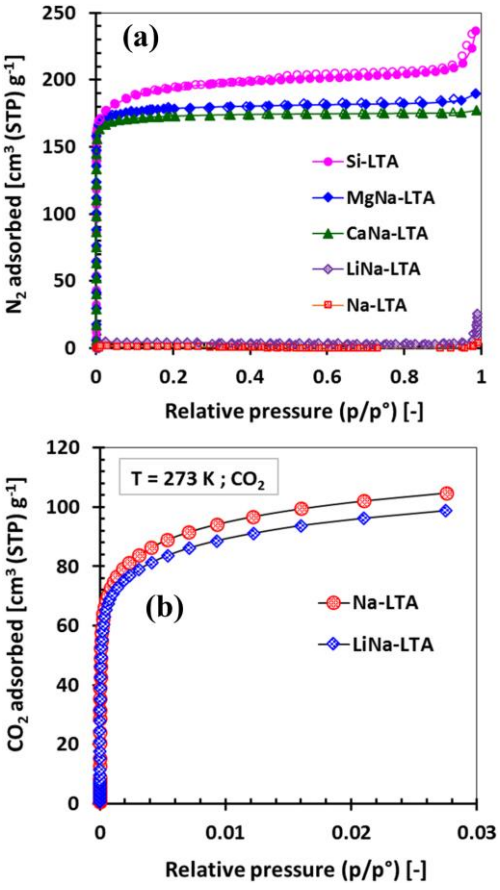

Figure 5. (a) N_2 adsorption-desorption isotherms measured at 77 K on studied adsorbents and (b) CO_2 adsorption isotherm measured at 273 K on the zeolites Na- and LiNa-LTA. The lines are guides to the eye.

Of particular interest is the significant difference in the rates of adsorption of propylene and propane exhibited by some monovalent cationic zeolites and thus, their potential as adsorbents for the kineticbased separation of C_3 hydrocarbons.

According to Fig. 7, the differences in uptake between propylene and propane of the adsorbents are striking; Na- and LiNa-LTA zeolites stand out by their high discrimination between the two adsorbates and ability to exclude essentially C_3H_8 molecules from entering their pore structure. It would, however, appear that the introduction of Li^+ cations within the structure of Na-LTA zeolite have improved the propylene uptake rate since a shorter time was necessary to attain equilibrium as compared with Na-LTA zeolite (16 min vs. 7 min for Na- and NaLi-LTA, respectively). Due to the size of Li^+ cations being smaller than Na^+ cations, the propylene diffusion rate in LiNa-LTA zeolite

is five times faster than that found for Na-LTA zeolite, which contains only Na^+ cations. However, it remains slowest against the significant increase in the diffusion of guest molecules as the monovalent Na^+ cations are substituted by the divalent Mg^{2+} and Ca^{2+} cations, as seen in Table 2.

It is also shown from Fig. 7 that the transient fractional uptakes of propylene and propane obtained on the Mg^{2+} and Ca^{2+} forms of the Na-LTA zeolite are identical, giving rise to similar diffusion time constants for both gases (Table 2). This suggests that the 8-ring window in these forms is large enough to allow the smooth diffusion of propylene and propane under the experiment conditions (i.e., 0.1 bar and 303 K). All these observation are in line with the work of Schˆollner et al. [60], who found that the transport mechanism of small alkenes is modified through addition of blocking cations.

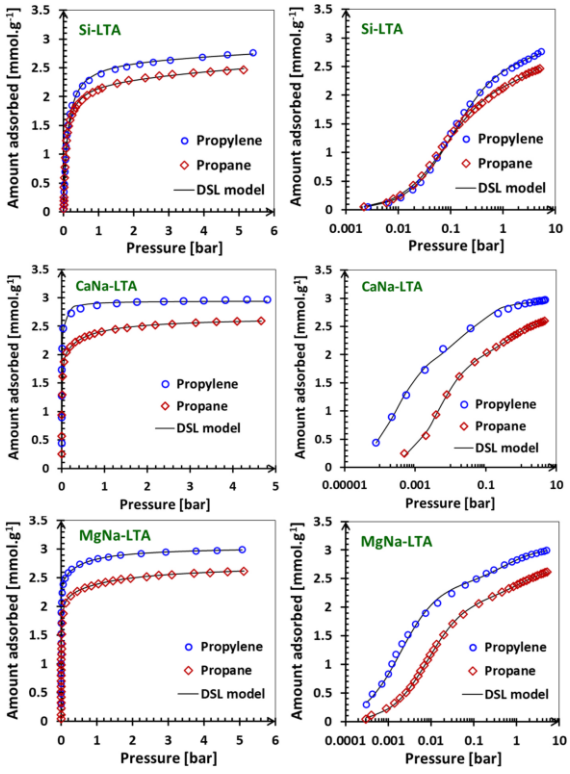

Figure 6. Propylene (circle) and propane (lozenge) adsorption isotherms on Si-, CaNa- and MgNa-LTA at 303 K in a linear-scale n vs p plot (left) and in a linear n vs logarithmic p-scale plot (right). Solid lines are DSL fit.

A well-known structure is CaNa-LTA of apparent composition $Na_{12-2x}Ca_xAl_{12}Si_{12}O_{48}$ with x varies from 0 to 6. In such an LTA structure, there are 8 type I sites (6-ring window), 3 type II sites (8-ring window), and 12 type III sites (4-ring window) [61]. When the value of x in $Na_{12-2x}Ca_xAl_{12}Si_{12}O_{48}$ is 4 or greater, which means that at least two-thirds of the Na^+ is replaced by Ca^{2+}, the material becomes 5 A zeolite because all type II sites (located in the pore-opening) are empty due to bivalent cations preference such as Sr^{2+}, Ca^{2+}, Mg^{2+}, and Zn^{2+} ions to occupy type I positions (6-ring window) [60,61]. On this basis, CaNa- and MgNa-LTA zeolites are found in this category of substitution and localization of cations, at least from a diffusion point of view. Consequently, the micropore diffusion, in zeolites with divalent cations, is maximized because none of the remaining Na^+ or Ca^{2+}, or Mg^{2+} cations do block the 8-ring pore window.

From the study carried out by R. Schoellner and U. Mueller [60]. On the zeolite Na-LTA, it was established that the strength of adsorptive centers in larger cavities (precisely, type I sites) and the diffusivity of small alkenes go in pair. As a result, it can be deduced that Mg^{2+} cations would interact strongly with propylene than Ca^{2+} cations as higher diffusion time constant in MgNa-LTA than in CaNa-LTA was noticed (Table 2).

As observed in Fig. 7, pure-silica zeolite appears to exhibit an intermediate behavior between the previous monovalent and bivalent structures. After about 1 min, C_3H_6 adsorption is 82% complete, while C_3H_8 adsorption is approximatively 25% complete. As seen from Table 2, the ratio of the diffusivity, propylene to propane for Si-LTA zeolite is 9 and 17 as estimated by Crank's model and LDF approximation, respectively, these values are lower than the ratio of purecomponent diffusivities of O_2/N_2 in the commercial separation of air using a carbon molecular sieve [62]. This proves the lack of performances of this adsorbent if it would be included in kinetic-based adsorption process (i.e., PSA).

Among the studied LTA zeolites, LiNa-LTA is the one standing out by its highest diffusivity ratio followed by Na-LTA zeolite, which rending it a good candidate to kinetically separate propylene from propane mixture. In this context, pressure (loading) and temperature dependences of diffusion coefficients were investigated. For this, a series of fractional uptakes of propylene on Na-LTA and LiNa-LTA were measured experimentally at three temperatures ranging from 323 to 373 K for an initial pressure of 0.5 bar (Fig. S8) following the same procedure as pointed out before. These results demonstrate that the adsorption uptake-time decreases with increasing temperature. As can be seen in Fig. S8, the predictions of Crank's model are in good agreement with the experimental kinetic data. By fitting Crank's model to the experimental kinetic adsorption curves available at various temperatures, the micropore diffusion time constants of propylene were estimated and summarized in Table S3.

From the data in Table 2, it can be inferred that an increase in adsorption temperature results in an increase in diffusion time coefficients because the diffusion of C_3H_6 molecular becomes quicker with temperature. This temperature dependence of transport diffusivity can be demonstrated by the Arrhenius equation represented by

$$K_{LDF} = \frac{D_c}{r_c^2} = A\ exp\left(\frac{-E_a}{RT}\right) \quad (14)$$

where E_a, A and R denote the activation energy, the Arrhenius factor and the gas constant, respectively. Equation (14) can be also written as,

$$\ln K_{LDF} = ln(D_c/r_c^2) = lnA - E_a/RT \quad (15)$$

From this equation (15), the activation energy (E_a) can be calculated from the slope of the plot between $ln(D_c/r_c^2)$ and the inverse of temperature ($1/T$), as illustrated in Fig. S9. The Arrhenius-type plot were linearly fitted with correlation coefficients (R2) more than 0.98, showing a good linearity between ln (Dc/r2c) and (1/ T). As a result of this fitting procedure, activation energies for propylene were found to be higher into Na-LTA pores than LiNa-LTA at the same pressure, i.e., 34.4 compared to 22.3 kJ mol^{-1} at 0.5 bar. This means that propylene can diffuse easier into LiNa-LTA than Na-LTA zeolite pores, which is consistent with the experimental data.

On the other hand, to elucidate the effect of pressure (loading) on molecular transport inside the monovalent (Na- and LiNa-LTA) zeolites, we have compared the diffusion time coefficients obtained by Crank's model, and reported in Table 2 and Table S3, regardless of the fact that these coefficients are not measured at the same temperature, but certainly for different pressures (i.e., 0.1 and 0.5 bar). It was found that the loading-dependent transport diffusivity decreased with the increase in pressure because the molecular diffusion resistance becomes larger with pressure.

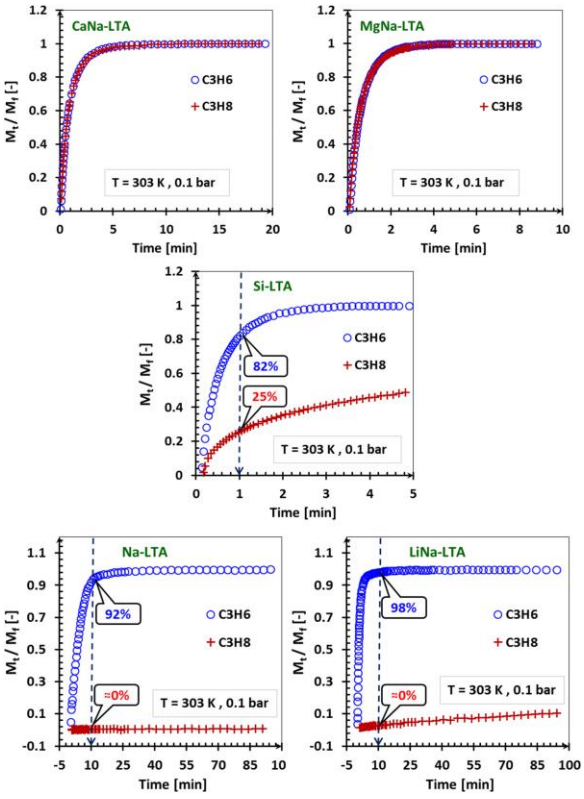

Figure 7. Adsorption kinetics curves for propylene (circle) and propane (cross) on CaNa-LTA, MgNa-LTA, Si-LTA, Na-LTA and LiNa-LTA at 303 K and from a reservoir pressure of 0.1 bar.

From a practical point of view, thermodynamic separation based on differences in affinities is preferable over the differences in rates of diffusion for a PSA-type application. One disadvantage of the latter separation mechanism is when the adsorption of the propylene is extremely slow, that makes pressure-swing adsorption inefficient by affecting the productivity. At this stage of discussion, it is mandatory to study the thermodynamic behavior of the adsorbed species in the five zeolites for a better ranking of their ability to separate propylene from propane. One way to do this is through the direct measurements of the released heat of adsorption as is addressed fully in the next section.

Table 2

Micropore diffusion time constants of propane and propylene on Si-, MgNa-, CaNa-, Na- and LiNa-LTA adsorbents at 303 K and 0.1 bar. LDF and Crank models were fitted to the experimental kinetic uptakes LDF: Linear Driving Force.

Adsorbent	LDF model		Crank model	
	$D_c/r_c^2\ (s^{-1}) \times 10^3$		$D_c/r_c^2\ (s^{-1}) \times 10^3$	
	propylene	propane	propylene	propane
Si-LTA	2.21	0.25	3.13	0.18
MgNa-LTA	2.05	2.03	2.57	2.43
CaNa-LTA	1.45	1.46	1.45	1.53
Na-LTA	0.25	/	0.31	/
LiNa-LTA	1.27	/	1.56	/

4.4 Thermodynamic analyses

The zero-coverage enthalpy, $\Delta\dot{h}_{ads}^{\theta=0}$, and Henry's constant, k_H, are two important thermodynamic properties, both of which characterize the interaction energy for a single molecule with the bare solid. In order to assess these thermodynamic properties for Si-, CaNa- and MgNa-LTA zeolites, single adsorption isotherms of both species of interest were first described by the DSL equation (see Fig. 6), then by applying equation (4), the Henry's constants were calculated. In addition to this, the adsorption enthalpies at zero-coverage for propylene and propane, $\Delta\dot{h}_{ads}^{\theta=0}$, were determined from the curves of the calorimetrically measured adsorption enthalpies as a function of adsorbed amounts (Fig. 8). Herein, two cases may be envisaged: (i) when the amount adsorbed, nads, is small enough to be considered similar to that at limit of zero loading, $\Delta\dot{h}_{ads}^{\theta=0}$ads can be taken as the first measured value of the released heat, otherwise (ii) we define a straight line from the two first measured heats of adsorption at very low loading. In this case, the intercept of this straight-line with the y-axis is the estimated zerocoverage enthalpy. The Henry's constants for the adsorption of propylene and propane on LTA materials together with their zero-coverage enthalpies are summarized in Table 3.

It can be seen that the enthalpy of adsorption (at zero-coverage) for C_3H_6 is marginally higher in the case of the MgNa-LTA zeolite than in the CaNa-LTA zeolite, indicating that Mg^{2+} cations interact strongly with C_3H_6. This confirms what was previously deduced from the assumption that diffusion rates and adsorption strength for alkenes, in general, goes together, as suggested by Schoellner and Mueller [60].

To the best of our knowledge, the experimental adsorption isotherms of propane and their corresponding adsorption enthalpies for Na-LTA and LiNa-LTA zeolites, to date, have not been reported at real equilibrium state and an ambient temperature. This may be because the experiments are an arduous and time-consuming process. However, enthalpies of propylene for Na-LTA and LiNa-LTA were successfully measured (see Fig. S7). It can be seen that the lithium adsorption centers in LiNa-LTA interact strongly with propylene as compared to that in Na-LTA (−76 vs. −65 kJ mol^{-1}). A similar observation was reported by C. Grande et al. [37] when they compared 13X zeolite to Li-exchanged 13X.

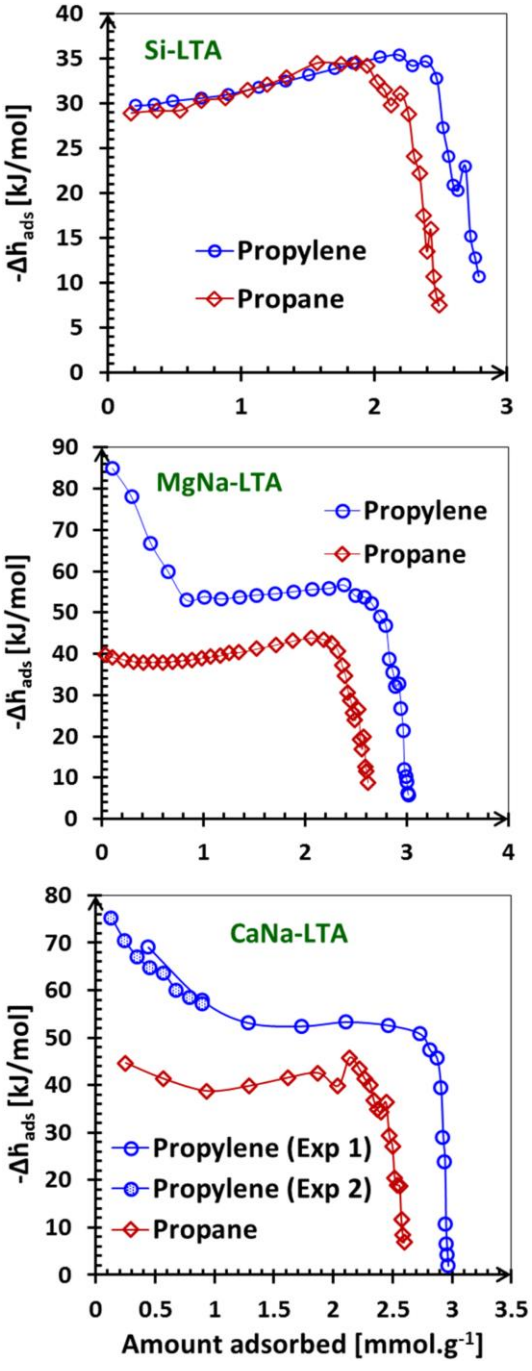

Figure 8. Adsorption enthalpy of C_3H_8 (lozenge) and C_3H_6 (circle) for Si-, CaNa-, Ca- and MgNa-LTA as a function of loading at 303 K.

For these monovalent zeolitic samples, unfortunately, the Henry's law constants cannot be accurately determined, and thus they are not included in Table 3, because it needs real equilibrium adsorption data for low pressure which have not been measured for propane. Therefore, any prediction of binary behavior can be questioned since the predictions are highly sensitive to Henry's constant [63].

Aside from the monovalent cationic zeolites, as seen in Table 3, Henry's law constants together with the pseudo-differential enthalpies at zero coverage are higher for the adsorption of propylene than for propane, except for Si-LTA (values were found to be similar), suggesting that the preferentially adsorbed gas is propylene. This is in good agreement with what was inferred previously from the comparison of isotherms data (Fig. 6).

In the literature, often, only the value for zero coverage, $\Delta\dot{h}_{ads}^{\theta=0}$, is calculated and discussed. However calorimetric measurements are necessary if the enthalpy of adsorption needs to be determined more accurately. In this regard, Grande et al. [64] studied the

adsorption of propane and propylene on 5 A zeolite (Grace Davison) in crystal as well as in pellet form. They found that the heat of adsorption is higher for propane over propylene by fitting the adsorption equilibrium isotherm data with Toth model. Mofarahi et al. [65] have also reported similar result for 5 A zeolite (CECA, in the form of pellets) by fitting the isotherm data with GM isotherm model [66]. On the other hand, in both studies, the equilibrium adsorption isotherms have showed a selectivity towards propylene. This discrepancy between the results can be assigned to not enough experimental data points collected at low loadings or the fact that they are extrapolated via the fitting procedure, which is strongly discouraged. This should increase the confidence of our direct calorimetric measurements (Table 3 and Fig. 8), which are in excellent consistency with what was inferred earlier from the comparison of isotherms data (Fig. 6).

Table 3
Pseudo-differential enthalpies at zero coverage ($\Delta\dot{h}_{ads}^{\theta=0}$) and Henry's constants of propylene ($k_{H,1}$) and propane ($K_{H,2}$) determined for Linde Type A (LTA) zeolites at 303 K.

Sample	$k_H[mol \cdot kg^{-1} \cdot bar^{-1}]$		$-\Delta\dot{h}_{ads}^{\theta=0}[kJ \cdot mol^{-1}]$	
	propylene	propane	propylene	propane
CaNa-LTA	7045	447	81	47
MgNa-LTA	1253	258	88	40
Si-LTA	24	28	30	29
Na-LTA	/	/	65	/
LiNa-LTA	/	/	76	/

To better evaluate the performance of the studied materials, we have also considered the enthalpy of adsorption over the entire adsorption range (not just at the limit of zero loading). Fig. 8 shows the calorimetrically measured heats of adsorption on three LTA zeolites plotted as a function of C_3H_6 and C_3H_8 loadings at 303 K. MgNa-LTA zeolite exhibits pronounced heterogeneity for the adsorption of C_3H_6. The heat of adsorption dropped sharply from −88 kJ mol^{-1} at the limit of zero loading to a value of −54 kJ mol^{-1} at low loading (n_{ads}= 0.8 mmol g^{-1}). This latter value (standing for the average value of the forward recorded enthalpies after 0.8 mmol g^{-1}) was maintained up to higher uptakes (2.4 mmol g^{-1}), before a substantial decrease indicating the end of the adsorption process. A similar trend was also observed for CaNa-LTA zeolite with the adsorption of C_3H_6 at least up to 1.4 mmol g^{-1}; the enthalpy in the Henry's Law limit is ~ −81 kJ mol^{-1} and then decreases gradually with increased adsorbate loadings (until 1.4 mmol g^{-1}) to finally levels off at a value of −54 kJ mol^{-1} at higher coverages. In short, from the previous energetic curves exposed in Fig. 8 for the adsorption of C_3H_6 on CaNa-LTA (or MgNa-LTA), it would appear like there is two blocks of data (i.e., a drastic decrease of heat of adsorption being less pronounced in the latter one, followed right after by significant similar values continue to a high adsorption capacity) that can be ascribed to the presence of different cations (Na^+ and either Ca^{2+} or Mg^{2+} cations) inside those zeolites. This is a typical behavior of microporous adsorbents indicating the presence of chemical heterogeneities or specific adsorption sites of various strengths.

Moreover, in both bivalent cationic zeolites, it's worth to note that the observed plateaus (around a value of −54 kJ mol^{-1} for the adsorption of C_3H_6, for example) are similar. It can be considered as a footprint of the interaction resulting from the presence of Na^+ cations within their framework if one take into account the homogenous energetic adsorption signature (a flat tendency for $\Delta\dot{h}_{ads}^{\theta=0}$, of C_3H_6 obtained on Na-LTA zeolite (Fig. S7).

The energetic decay, displayed by propylene in the above zeolites, is typical for heterogeneous systems. The initially high heat of adsorption can be ascribed to the π electrons of C_3H_6 molecule that directly interact with the charged cations on zeolite surfaces. As the loading increases, the 'lateral' interactions between molecules also increase which should normally result in an increasing adsorption enthalpy. On the other hand, the additional propylene molecules in the pores cannot approach the cations as closely which results in a decrease in the vertical interactions. For propylene in CaNa-LTA (or MgNa-LTA), as for most other heterogeneous systems, the decrease in vertical interactions overwhelm the increase in lateral interaction resulting in overall decay of adsorption enthalpy with coverage.

In all the energetic presented curves (Fig. 8) for all the studied samples in this work, a common drop for the enthalpies of adsorption were observed at the last stage of the adsorption process, whether with propylene or propane. This can be assigned to adsorption completion resulting in weakening of lateral interactions. In other words, as the amount adsorbed of gases relative to each dosing step decreases with increasing pressure, the released heat of adsorption corresponding to the adsorbate-adsorbate interaction becomes ever increasing low until the adsorption process ends.

As depicted in Fig. 8, however, the case for the adsorption of propylene and propane in the pure-silica zeolite is quite different. At first, it shows a constant enthalpy of adsorption (~−30 kJ mol^{-1}) and then progressively increases until reach a maximum at high coverage. This implies that the surface and porous structure of Si-LTA are energetically homogeneous. This is expected as the pure-silica zeolite

does not possess specific sites even with propylene as an unsaturated hydrocarbon. Also, it is noteworthy that the stark difference between the enthalpy of adsorption of propylene and propane on MgNa-LTA, displayed in Fig. 8, is a clear indication that heterogeneity (and homogeneity observed with propane) is related to a system and not to a solid only.

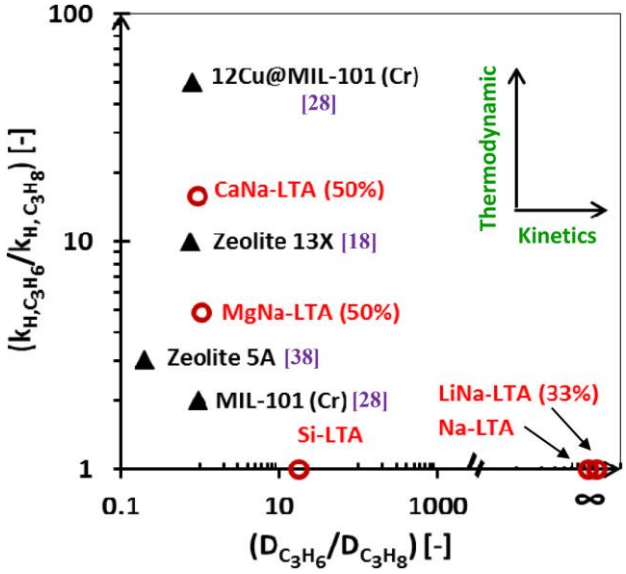

Figure 9. Comparison of Henry's constants of propylene over propane versus the ratio of their diffusivities on several adsorbents (full triangle) with the synthesized adsorbents in the present work (circles) at T = 303 K. References are shown in brackets. In parenthesis is the exchange rate.

In order to rank the materials considered in this study, and make a comparison with other results available in the literature [18,28,38,64], a plot of Henry's constants of propylene over propane versus the ratio of their diffusivities can be proposed (Fig. 9). This plot enables to identify which materials can be better suited to thermodynamic or kinetic separation of the C_3 molecules considered here. It is worth to note that the ratio of Henry's constants is a simple parameter to find the equilibrium selectivity at low pressures, while the ratio of diffusivities defines the kinetic selectivity.

As can be interpreted from Fig. 9, CaNa- and MgNa-LTA are capable of thermodynamically separate propylene from propane, whereas Na- and LiNa-LTA are capable of kinetically separate them. It also shows that the highest ratio for Henry's constants is in favor of copper-loaded within MIL-101(Cr) (12Cu@MIL-101(Cr)) [28]. However, by slightly increasing pressure, the selectivity decreases until reaching to value of 10, as stated by H. Abedini et al. [28]. On the other hand, the CaNa-LTA zeolite stands out most of its competitors for the adsorptive separation of propane/propylene mixtures and can be enhanced by increasing pressure to be better than 12Cu@MIL-101(Cr). Indeed, the presence of calcium (Ca^{2+}) cations within its framework promotes thermodynamic to a dominant role. The same separation mechanism was found on MgNa-LTA zeolite, which showed a moderate limiting selectivity (~4.9) but clearly higher than that of the commercial 5 A zeolite [38].

At this point, we want to draw attention to the discrepancy that lies in higher IAST selectivity values for zeolites with bivalent cations as compared to that of the commercial 5 A zeolite (in the form of crystals) [38]. By knowing that the partially exchanged zeolites with Ca^{2+} and Mg^{2+} are type 5 A (Ca-LTA) with rather unobstructed and larger windows, as mentioned previously, the paradox in SIAST values may be mainly ascribed to the accuracy of equilibria data at low pressure domain (i.e., lack of information at Henry's region and/or problems related to fit procedure). Also, the differences related to the diffusivity ratio can be explained by the use of different crystal sizes. Apart from the bivalent cationic zeolites that show a thermodynamic behavior, the insertion of monovalent cations in LTA zeolite structure (in our case LiNa- and Na-LTA) hinders the propane from entering their structures resulting into a dominant kinetic mechanism.

As commented in previous sections, Si-LTA can be withdrawn from this set of zeolites due its inadequate separation performances (i.e., selectivity at limit of zero coverage is close to unity with low diffusivities ratio).

4.5 Thermodynamic analyses

To test the applicability of adsorbents for a PSA process to separate propylene□ propane mixture and predict favorable operating

conditions, IAST selectivity of propylene over propane was predicted as a function of feed composition over four different total pressures, 1, 3, 5 and 8 bar, and temperature T = 303 K using the validated IAST solver. Depending on the application required for the C3 separation, the ratio of propylene to propane in the mixture can vary according to cracking conditions for example. However, for numerical comparison of IAST selectivity, three bulk phase mole fractions were selected: an equimolar propylene/propane mixture (Feed-1) represents steam cracker off gas, propane-rich feed consisting of 85% of propane and 15% propylene (Feed-2), and finally propylene rich feed with 85% of propylene and balance propane representing fluid catalytic cracker (FCC) off gas (Feed-3).

Calculated propylene/propane selectivity from the IAST for mixed cation exchanged LTA materials contrasted with their pure-silica analogue is presented in Fig. 10. At a given feed composition. The IAST predicts that propylene/propane selectivity for CaNa-LTA at 303 K increases with pressure (see Fig. S4). Particularly, a selectivity value of 23 is obtained for Feed-2 with IAST at 8 bar and 303 K, whereas the corresponding value for Feed-3 is 27. These values are the highest selectivity ones obtained among the three adsorbents reported in this section, suggesting that for PSA/VSA based propylene/propane separation at higher pressure, CaNa-LTA may be a good adsorbent material. The IAST selectivity, SIAST, predicts that the propylene/propane selectivity for MgNa-LTA also changes with pressure in similar way (Fig. S4), although the numerical values of the selectivity are different from CaNa-LTA. For Feed-3, the IAST selectivity appears to be slightly more affected with increase in pressure in the latter zeolite than in the former case. It may be because the isotherm parameters for n0 propylene and propane are comparable in the case of CaNa-LTA, whereas in the case of MgNa-LTA, the n0 for propylene is higher than for propane. From IAST calculations in Fig. 10, it can also be inferred that the IAST selectivity of zeolite Si-LTA, close to unity, is almost independent of bulk phase concentration (Feed-1 to 3) and pressure at 303 K.

Fig. 11 represents propylene enrichment curves calculated for the selected set of cation-exchanged materials as well as their pure silica zeolite by the IAST. The enrichment of the adsorbed phase in propylene decreases in the order CaNa- > MgNa- > Si-LTA, opposite to the adsorption strength.

During the design of a propylene/propane PSA separation process utilizing cationic LTA zeolites, a compromise between selectivity, diffusivity and working capacity would appear to be necessary. As for example the case for the adsorption separation of ethylene from ethane on Na-ETS; although it has a high selectivity, the swing capacity for both adsorbed species is low, which make this adsorbent difficult to be implemented in PSA, reported by Al-Baghli and Loughlin [67]. Likewise, in our work, Na-LTA presents a moderate capacity towards propylene together with a high kinetic selectivity, but their very slow diffusion at ambient temperature makes this adsorbent impractical for PSA scheme, as confirmed by J. G. Min et al. [68] through breakthrough experiments.

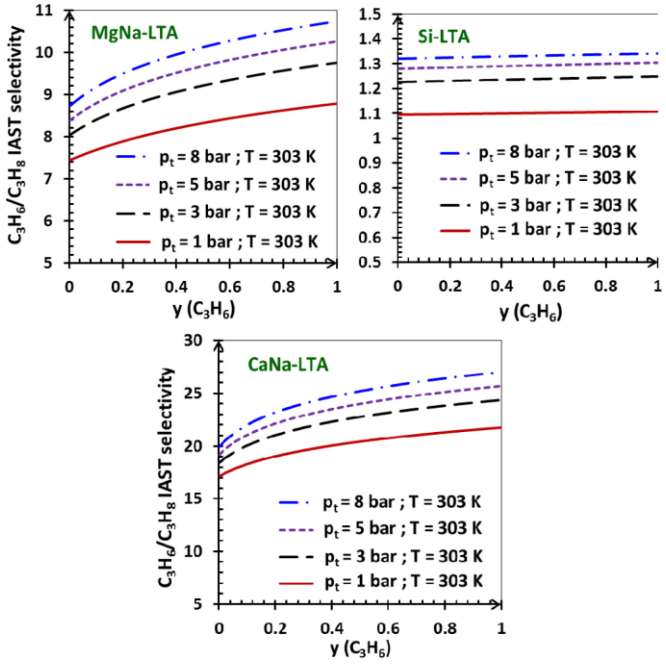

Figure 10. IAST calculations for the adsorption selectivity for binary C_3H_6/C_3H_8 mixtures as a function of the bulk phase mole fraction of C_3H_6, y, on Si-LTA, MgNa-LTA and CaNa-LTA. The calculations are presented for four different total pressures, p_t, as follows: 1 bar (solid line), 3 bar (long dashed line), 5 bar (dotted line), 8 bar (dot dashed line) at 303 K.

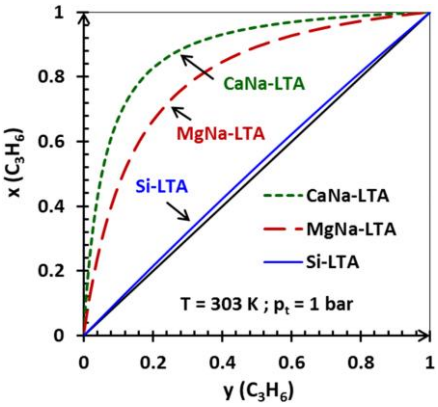

Figure 11. Phase diagram (x vs. y for C_3H_6) of equimolar binary mixture of propylene and propane at constant total pressure and temperature (p_t = 1 bar and T = 303 K) for three zeolites: CaNa- (dashed line), MgNa- (long dashed line) and Si-LTA (solid line). The fitted model to all the obtained adsorption isotherms for both gases is DSL.

However, unlike Na-LTA zeolite, we have shown that mixed cationic forms, e.g. MgNa-LTA and CaNa-LTA, would be good candidates for propylene/propane adsorption separation, even though the cation composition ratio in these adsorbents might not be optimal. Also, we would put emphasis on the fact that intermediate adsorption characteristics and better fulfill the requirements for a wide range of PSA processes should be possible by vary continuously the compositional ratio of the cations.

5. Conclusions

In this study, five adsorbents of type A zeolitic structure have been proposed for separation of propane/propylene mixtures by adsorption. These adsorbents are the lab synthesized pure-silica zeolite (Si-LTA, also known as ITQ-29) and the raw aluminosilicate zeolite (Na-LTA, also known as 4 A). From the latter zeolite, we have prepared three new adsorbents by ion exchange process, namely, LiNa-, CaNa-, and MgNa-LTA. All these zeolites were successfully characterized by PXRD, gas adsorption measurement, TGA, XRF, SEM and EDX mapping. To evaluate the performance of those synthesized samples, pure component adsorption equilibrium isotherms of propane and propylene were experimentally measured at 303 K and pressures up to 5 bar. The isotherms were well described by dual-site Langmuir equation over the entire range of pressure, especially at low pressure as confirmed by plotting the adsorption data in semi-logarithmic scale. By an accurate fitting of the isothermal micropore model (Crank's model) to the experimental uptake curves, diffusion time constants of the adsorbates were also estimated. These results are found to be in excellent agreement with those derived from the LDF approximativte solution model, indicating that intracrystalline diffusion is the limiting rate of the mass trasfert within the channels of zeolite microcrystals. This study about the characteristics (both kinetic and thermodynamic) of the propylene and propane adsorption on a set of LTA zeolites highlights that the separation performances (which involve kinetic separation, exclusion (i.e., the extreme case of diffusion) and equilibrium separation) can be tuned quite precisely by cation exchange process. The monovalent cationic zeolites were found to be able to kinetically separate propylene, being more practical with LiNa-LTA zeolite since C_3H_6 diffuses faster than in Na-LTA while keeping C_3H_8 outside the framework. The bivalent cationic zeolites show an equilibrium separation, for which the IAST was used to evaluated its ability. Although the highest propylene/propane IAST selectivity (nearly 15 at the limit of zero pressure) was found with the CaNa-LTA, the Mg-containing zeolite (at 50% only), which gave a minimum of 5 selectivity, can also be a potential sorbent in targeted separation whatever the molar composition mixture. Also, except the pure-silica zeolite (Si-LTA) which shows a moderate kinetic separation, these materials could be appropriate adsorbents for the separation of propylene from propane by pressure swing adsorption although there are still other criteria (reversibility and reusability) needed to be assessed for an adsorbent to be efficient. Finally, we would like to draw interest to the fact that calorimetry data are reported for the first time in this document contributing to enrich literature for future purposes, including modelling of scheme followed by a design of adsorber columns for pressure swing adsorption process.

CRediT authorship contribution statement

Mohammed-El Amine Benchaabane: Writing – original draft, Methodology, Investigation. Gabriel Trierweiler Goncalves: Methodology, Investigation. Emily Bloch: Supervision. Jean-Louis Paillaud: Supervision. T. Jean Daou: Funding acquisition, Conceptualization. Sandrine Bourrelly: Writing – review & editing, Supervision. Gérald Chaplais: Writing – review & editing, Supervision, Project administration. Philip L. Llewellyn: Writing – review & editing, Supervision.

Declaration of competing interest

The authors declare that they have no known competing financial interests or personal relationships that could have appeared to influence the work reported in this paper.

Data availability

Data will be made available on request.

Acknowledgements

The authors acknowledge French National Research Agency (ANR) for the financial support to SAAMM project (ANR-20-CE07-0033) and the Ecole Militaire Polytechnique of Alger for the scholarship granted to Mr. Mohammed-El Amine Benchaabane.

Appendix A. Supplementary data

Supplementary data to this article can be found online at https://doi.org/10.1016/j.micromeso.2022.112211.

References

[1] H. Järvelin, J.R. Fair, Adsorptive separation of propylene-propane mixtures, Ind. Eng. Chem. Res. 32 (10) (1993) 2201–2207, https://doi.org/10.1021/ie00022a001.

[2] D.S. Sholl, R.P. Lively, Comment, Nature 532 (435) (2016) 6–9.

[3] R.B. Eldridge, Olefin/paraffin separation technology: a review, Ind. Eng. Chem. Res. 32 (10) (1993) 2208–2212, https://doi.org/10.1021/ie00022a002.

[4] S.U. Rege, J. Padin, R.T. Yang, Olefin/paraffin separations by adsorption: π-complexation vs. Kinetic separation, AIChE J. 44 (4) (1998) 799–809, https://doi.org/10.1002/aic.690440405.

[5] V. Gokhale, S. Hurowitz, J.B. Riggs, A comparison of advanced distillation control techniques for a propylene/propane splitter, Ind. Eng. Chem. Res. 34 (12) (1995) 4413–4419, https://doi.org/10.1021/ie00039a033.

[6] H.S. Papastathopoulou, W.L. Luyben, Control of a binary sidestream distillation column, Ind. Eng. Chem. Res. 30 (4) (1991) 705–713, https://doi.org/10.1021/ie00052a013.

[7] C.A. Grande, A.E. Rodrigues, Propane/propylene separation by Pressure Swing Adsorption using zeolite 4A, Ind. Eng. Chem. Res. 44 (23) (2005) 8815–8829, https://doi.org/10.1021/ie050671b.

[8] C.A. Grande, F. Poplow, A.E. Rodrigues, Vacuum pressure swing adsorption to produce polymer-grade propylene, Separ. Sci. Technol. 45 (9) (2010) 1252–1259, https://doi.org/10.1080/01496391003652767.

[9] C.A. Grande, Advances in pressure swing adsorption for gas separation, ISRN Chem. Eng. 2012 (2012) 1–13, https://doi.org/10.5402/2012/982934.

[10] T.(United S, Oak Ridge National Lab. (ORNL), Oak Ridge, “Materials for Separation Technologies, Energy and Emission Reduction Opportunities, United States, 2005, https://doi.org/10.2172/1218755.

[11] P. Pullumbi, F. Brandani, S. Brandani, Gas separation by adsorption: technological drivers and opportunities for improvement, Curr. Opin. Chem. Eng. 24 (June) (2019) 131–142, https://doi.org/10.1016/j.coche.2019.04.008.

[12] D. Ruthven, Principle of Adsorption Process, 1984, p. 454.

[13] P.C. Wankat, Separation Process Engineering 49 (2004) 11.

[14] S. Sircar, T.C. Golden, M.B. Rao, Activated carbon for gas separation and storage, Carbon N. Y. 34 (1) (1996) 1–12, https://doi.org/10.1016/0008-6223(95)00128-X.

[15] H. Abdi, H. Maghsoudi, All-silica DD3R zeolite for adsorptive separation of propylene from propane: equilibrium and kinetic data,

Microporous Mesoporous Mater. 307 (July) (Nov. 2020), 110513, https://doi.org/10.1016/j.micromeso.2020.110513.

[16] P. Sá Gomes, N. Lamia, A.E. Rodrigues, Design of a gas phase simulated moving bed for propane/propylene separation, Chem. Eng. Sci. 64 (6) (2009) 1336–1357, https://doi.org/10.1016/j.ces.2008.11.022.

[17] W.C. Kuah, S. Effendy, S. Farooq, Industrial scale propylene/propane separation using pressure vacuum swing adsorption, Ind. Eng. Chem. Res. 57 (18) (2018), https://doi.org/10.1021/acs.iecr.8b00289.

[18] F.A. Da Silva, A.E. Rodrigues, Adsorption equilibria and kinetics for propylene and propane over 13X and 4A zeolite pellets, Ind. Eng. Chem. Res. 38 (5) (1999) 2051–2057, https://doi.org/10.1021/ie980640z.

[19] C.A. Grande, E. Rodrigues, Silica Gel, Van Nostrand's Sci. Encycl., 2007, pp. 1686–1693, https://doi.org/10.1002/0471743984.vse9038.

[20] C.A. Grande, S. Cavenati, F.A. Da Silva, Adsorption, 2005, pp. 7218–7227.

[21] J. Liu, et al., New carbon molecular sieves for propylene/propane separation with high working capacity and separation factor, Carbon N. Y. 123 (Oct. 2017) 273–282, https://doi.org/10.1016/j.carbon.2017.07.068.

[22] H. Maghsoudi, H. Abdi, A. Aidani, Temperature- A nd pressure-dependent adsorption equilibria and diffusivities of propylene and propane in pure-silica Si-CHA zeolite, Ind. Eng. Chem. Res. 59 (4) (2020) 1682–1692, https://doi.org/10.1021/acs.iecr.9b05451.

[23] B.L. Newalkar, N.V. Choudary, P. Kumar, S. Komarneni, T.S.G. Bhat, Exploring the potential of mesoporous silica, SBA-15, as an adsorbent for light hydrocarbon separation, Chem. Mater. 14 (1) (2002) 304–309, https://doi.org/10.1021/cm0106466.

[24] X. Wang, et al., Guest-dependent pressure induced gate-opening effect enables effective separation of propene and propane in a flexible MOF, Chem. Eng. J. 346 (2018) 489–496, https://doi.org/10.1016/j.cej.2018.03.163.

[25] H. Wang, et al., Tailor-made microporous metal–organic frameworks for the full separation of propane from propylene through selective size exclusion, Adv. Mater. 30 (49) (Dec. 2018) 1–9, https://doi.org/10.1002/adma.201805088.

[26] P. Krokidas, et al., ZIF-67 framework: a promising new candidate for propylene/propane separation. Experimental data and molecular simulations, J. Phys. Chem. C 120 (15) (2016) 8116–8124, https://doi.org/10.1021/acs.jpcc.6b00305.

[27] E.I. Basaldella, J.C. Tara, G.A. Armenta, M.E.P. Iglesias, Cu/SBA-15 as adsorbent for propane/propylene separation, J. Porous Mater. 14 (3) (2007) 273–278, https://doi.org/10.1007/s10934-006-9062-6.

[28] H. Abedini, A. Shariati, M.R. Khosravi-Nikou, Separation of propane/propylene mixture using MIL-101(Cr) loaded with cuprous oxide nanoparticles: adsorption equilibria and kinetics study, Chem. Eng. J. 387 (January) (May 2020), 124172, https://doi.org/10.1016/j.cej.2020.124172.

[29] E.I. Basaldella, J.C. Tara, G.A. Armenta, M.E. Patiño-Iglesias, E.R. Castellón, Propane/propylene separation by selective olefin adsorption on Cu/SBA-15 mesoporous silica, J. Sol. Gel Sci. Technol. 37 (2) (2006) 141–146, https://doi.org/10.1007/s10971-006-6434-y.

[30] J. Padin, S.U. Rege, R.T. Yang, L.S. Cheng, Molecular sieve sorbents for kinetic separation of propane/propylene, Chem. Eng. Sci. 55 (20) (2000) 4525–4535, https://doi.org/10.1016/S0009-2509(00)00099-3.

[31] D.J. Safarik, R.B. Eldridge, Olefin/paraffin separations by reactive absorption: a review, Ind. Eng. Chem. Res. 37 (7) (1998) 2571–2581, https://doi.org/10.1021/ie970897h.

[32] Y. Sung Park, Y. Soo Kang, S. Wook Kang, Cost-effective facilitated olefin transport membranes consisting of polymer/AgCF3SO3/Al(NO3)3 with long-term stability, J. Membr. Sci. 495 (3) (2015) 61–64, https://doi.org/10.1016/j.memsci.2015.07.061.

[33] David H. Olson, Light hydrocarbon separation using 8-Member ring zeolites, US Patent No 6 (488) (2002) 741.

[34] M.J. den Exter, J.C. Jansen, H. van Bekkum, Separation of permanent gases on the all-silica 8-ring clathrasil DD3R, Stud. Surf. Sci. Catal. 84 (C) (1994) 1159–1166, https://doi.org/10.1016/S0167-2991(08)63653-8.

[35] A. Corma, F. Rey, J. Rius, M.J. Sabater, S. Valencia, Supramolecular self-assembled molecules as organic directing agent for synthesis of zeolites, Nature 431 (7006) (2004) 287–290, https://doi.org/10.1038/nature02909.

[36] N. Hedin, G.J. DeMartin, W.J. Roth, K.G. Strohmaier, S.C. Reyes, PFG NMR selfdiffusion of small hydrocarbons in high silica DDR, CHA and LTA structures, Microporous Mesoporous Mater. 109 (1–3) (2008) 327–334, https://doi.org/10.1016/j.micromeso.2007.05.007.

[37] C.A. Grande, J. Gascon, F. Kapteijn, A.E. Rodrigues, Propane/propylene separation with Li-exchanged zeolite 13X, Chem. Eng. J. 160 (1) (2010) 207–214, https://doi.org/10.1016/j.cej.2010.03.044.

[38] S. Divekar, et al., Adsorption equilibria of propylene and propane on zeolites and prediction of their binary adsorption with the ideal adsorbed solution theory, J. Chem. Eng. Data 61 (7) (2016), https://doi.org/10.1021/acs.jced.6b00294.

[39] R.T. Yang, Adsorbents: Fundamentals and Applications, Wiley-Interscience, 2003.

[40] Z. Tahraoui, H. Nouali, C. Marichal, P. Forler, J. Klein, T.J. Daou, Influence of the compensating cation nature on the water adsorption properties of zeolites, Molecules 25 (4) (2020), https://doi.org/10.3390/molecules25040944.

[41] Y. Bouizi, J.L. Paillaud, L. Simon, V. Valtchev, Seeded synthesis of very high silica zeolite A, Chem. Mater. 19 (4) (2007) 652–654, https://doi.org/10.1021/cm063019v.

[42] P.L. Llewellyn, G. Maurin, Gas adsorption microcalorimetry and modelling to characterise zeolites and related materials, Compt. Rendus Chem. 8 (3–4) (2005) 283–302, https://doi.org/10.1016/j.crci.2004.11.004.

[43] D.D. Do, Adsorption analysis: Equilibria and kinetics, vol. 2, Imperial College Press, 1998.

[44] G.M.J. Rouquerol, F. Rouquerol, K.S.W. Sing, P. Llewellyn, Adsorption by Powders and Porous Solids, 2014.

[45] K.N. Son, G.E. Cmarik, J.C. Knox, J.A. Weibel, S.V. Garimella, Measurement and prediction of the heat of adsorption and equilibrium concentration of CO_2 on zeolite 13X, J. Chem. Eng. Data 63 (5) (2018) 1663–1674, https://doi.org/10.1021/acs.jced.8b00019.

[46] L.N. Bell, Thermodynamics of photosynthesis, Biophysics 9 (3) (1964) 316–321.

[47] D.M. Ruthven, Sorption kinetics for diffusion-controlled systems with a strongly concentration-dependent diffusivity, Chem. Eng. Sci. 59 (21) (2004) 4531–4545, https://doi.org/10.1016/j.ces.2004.06.028.

[48] D.M. Ruthven, K.F. Loughlin, The effect of crystallite shape and size distribution on diffusion measurements in molecular sieves, Chem. Eng. Sci. 26 (5) (1971) 577–584, https://doi.org/10.1016/0009-2509(71)86002-5.

[49] E. Glueckauf, Theory of chromatography. Part V. Separation of two solutes following a Freundlich isotherm, J. Chem. Soc. (1947) 1321–1329, https://doi.org/10.1039/jr9470001321.

[50] E.I. Unuabonah, M.O. Omorogie, N.A. Oladoja, Modeling in Adsorption: Fundamentals and Applications, Elsevier Inc., 2019.

[51] M. Siahpoosh, S. Fatemi, A. Vatani, Mathematical modeling of single and multicomponent adsorption fixed beds to rigorously predict the mass transfer zone and breakthrough curves, Iran. J. Chem. Chem. Eng. 28 (3) (2009) 25–44, https://doi.org/10.30492/ijcce.2009.6844.

[52] Y. Marcus, A simple empirical model describing the thermodynamics of hydration of ions of widely varying charges, sizes, and shapes, Biophys. Chem. 51 (2–3) (1994) 111–127, https://doi.org/10.1016/0301-4622(94)00051-4.

[53] F. Collins, A. Rozhkovskaya, J.G. Outram, G.J. Millar, A critical review of waste resources, synthesis, and applications for Zeolite LTA, Microporous Mesoporous Mater. 291 (August 2019) (2020), 109667, https://doi.org/10.1016/j.micromeso.2019.109667.

[54] S. Tanaka, et al., Adsorption and diffusion phenomena in crystal size engineered ZIF-8 MOF, J. Phys. Chem. C 119 (51) (2015) 28430–28439, https://doi.org/10.1021/acs.jpcc.5b09520.

[55] T.H. Bae, J. Liu, J.A. Thompson, W.J. Koros, C.W. Jones, S. Nair, Solvothermal deposition and characterization of magnesium hydroxide nanostructures on zeolite crystals, Microporous Mesoporous Mater. 139 (1–3) (2011) 120–129,

https://doi.org/10.1016/j.micromeso.2010.10.028.

[56] F. Benaliouche, N. Hidous, M. Guerza, Y. Zouad, Y. Boucheffa, Characterization and water adsorption properties of Ag- and Zn-exchanged A zeolites, Microporous Mesoporous Mater. 209 (2015) 184–188, https://doi.org/10.1016/j.micromeso.2014.10.039.

[57] M. Thommes, et al., Physisorption of gases, with special reference to the evaluation of surface area and pore size distribution (IUPAC Technical Report), Pure Appl. Chem. 87 (9–10) (2015) 1051–1069, https://doi.org/10.1515/pac-2014-1117.

[58] R. Bardestani, G.S. Patience, S. Kaliaguine, Experimental methods in chemical engineering: specific surface area and pore size distribution measurements—BET, BJH, and DFT, Can. J. Chem. Eng. 97 (11) (2019) 2781–2791, https://doi.org/10.1002/cjce.23632.

[59] M.E. Patiño-Iglesias, G. Aguilar-Armenta, A. Jiménez-López, E. Rodríguez-Castellón, Kinetics of the total and reversible adsorption of propylene and propane on zeolite 4A (CECA) at different temperatures, Colloids Surfaces A Physicochem. Eng. Asp. 237 (1–3) (2004) 73–77, https://doi.org/10.1016/j.colsurfa.2004.02.005.

[60] R. Schoellner, U. Mueller, In crack-gasesfluence of mono- and bivalent cations in 4A-zeolites on the adsorptive separation of ethene and propene from, Adsorpt. Sci. Technol. 3 (3) (1986) 167–171, https://doi.org/10.1177/026361748600300306.

[61] N. Hedin, G.J. DeMartin, K.G. Strohmaier, S.C. Reyes, PFG NMR self-diffusion of propylene in ITQ-29, CaA and NaCaA: window size and cation effects, Microporous Mesoporous Mater. 98 (1–3) (2007) 182–188, https://doi.org/10.1016/j.micromeso.2006.08.017.

[62] T. Mixtures, C.M. Sieve, Oxygen, Nitrogen and Their Mixtures, vol. 40, 1994, pp. 577–585, 4.

[63] O. Talu, Needs, status, techniques and problems with binary gas adsorption experiments, Adv. Colloid Interface Sci. 76 (77) (1998) 227–269, https://doi.org/10.1016/S0001-8686(98)00048-7.

[64] C.A. Grande, C. Gigola, A.E. Rodrigues, Adsorption of propane and propylene in pellets and crystals of 5A zeolite, Ind. Eng. Chem. Res. 41 (1) (2002) 85–92, https://doi.org/10.1021/ie010494o.

[65] M. Mofarahi, M. Sadrameli, J. Towfighi, Four-bed vacuum pressure swing adsorption process for propylene/propane separation, Ind. Eng. Chem. Res. 44 (5) (2005) 1557–1564, https://doi.org/10.1021/ie034016k.

[66] U. von Gemmingen, A new approach to adsorption isotherms, Gas Sep. Purif. 7 (3) (1993) 175–181, https://doi.org/10.1016/0950-4214(93)80007-J.

[67] N.A. Al-baghli, K.F. Loughlin, T. Background, Binary and ternary adsorption of methane, ethane, and ethylene on titanosilicate, ETS-10 Zeolite 1 (2006) 248–254, https://doi.org/10.1021/je050364c.

[68] J.G. Min, K.C. Kemp, S.B. Hong, Propylene/propane separation on a ferroaluminosilicate levyne zeolite, Microporous Mesoporous Mater. 294 (August 2019) (2020), 109833, https://doi.org/10.1016/j.micromeso.2019.109833.